

Application of Green-enhanced Nano-lantern as a bioluminescent ratiometric indicator for measurement of *Arabidopsis thaliana* root apoplastic fluid pH

Quang Tran^{1,2}  | Kenji Osabe^{1,2} | Tetsuyuki Entani¹ | Tetsuichi Wazawa¹ | Mitsuru Hattori^{1,2} | Takeharu Nagai^{1,2} 

¹SANKEN (The Institute of Scientific and Industrial Research), Osaka University, Ibaraki, Japan

²Department of Biotechnology, Graduate School of Engineering, Osaka University, Suita, Japan

Correspondence

Takeharu Nagai, SANKEN (The Institute of Scientific and Industrial Research), Osaka University, 8-1, Mihogaoka, Ibaraki 567-0047, Japan.

Email: ng1@sanken.osaka-u.ac.jp

Funding information

Plant Transgenic Design Initiative; Japan Society for the Promotion of Science; Japan Science and Technology Agency

Abstract

Plant root absorbs water and nutrients from the soil, and the root apoplastic fluid (AF) is an important intermediate between cells and the surrounding environment. The acid growth theory suggests that an acidic AF is needed for cell wall expansion during root growth. However, technical limitations have precluded the quantification of root apoplastic fluid pH (AF-pH). Here, we used Green-enhanced Nano-lantern (GeNL), a chimeric protein of the luciferase NanoLuc (Nluc) and the green fluorescent protein mNeonGreen (mNG), as a ratiometric pH indicator based on the pH dependency of bioluminescence resonance energy transfer efficiency from Nluc to mNG. Luminescence spectrum of GeNL changed reciprocally from pH 4.5 to 7.5, with a pK_a of 5.5. By fusing GeNL to a novel signal peptide from *Arabidopsis thaliana* Cellulase 1, we localised GeNL in *A. thaliana* AF. We visualised AF dynamics at subcellular resolution over 30 min and determined flow velocity in the maturation zone to be $0.97 \pm 0.06 \mu\text{m/s}$. We confirmed that the developing root AF is acidic in the pH range of 5.1–5.7, suggesting that the AF-pH is tightly regulated during root elongation. These results support the acid growth theory and provide evidence for AF-pH maintenance despite changes in ambient pH.

KEYWORDS

bioluminescence, pH homeostasis, pH indicator, root imaging, apoplast

Summary statement

We visualised and quantified the pH dynamics by localising a bioluminescent ratiometric indicator to the root apoplastic fluid (AF) of *Arabidopsis thaliana*. The AF-pH was dynamically acidified as the root developed regardless of different ambient pH, suggesting a strict regulation of AF-pH.

Quang Tran and Kenji Osabe contributed equally to this study.

This is an open access article under the terms of the Creative Commons Attribution-NonCommercial-NoDerivs License, which permits use and distribution in any medium, provided the original work is properly cited, the use is non-commercial and no modifications or adaptations are made.

© 2022 The Authors. *Plant, Cell & Environment* published by John Wiley & Sons Ltd.

1 | INTRODUCTION

The pH of soil or growth medium can affect plant growth and development (Walter et al., 2000). The root apoplast, which includes the cell wall and the space outside the plasma membrane, is the first barrier exposed to the outside environment (Figure 1). The root cell wall, mostly made up of cellulose, hemicellulose and pectin, has pores that allow water and solutes from soil or growth medium to enter the extracellular space, which is filled with apoplastic fluid (AF) (Carpita et al., 1979). Thus, the apoplastic fluid pH (AF-pH) is thought to be influenced by the medium pH. To protect themselves from changes in medium pH, root cells can regulate the extracellular pH through H^+ -ATPase to maintain the function of biological molecules, including enzymes for root growth (Elmore & Coaker, 2011; Falhof et al., 2016; Geilfus, 2017; Kesten et al., 2019; Li et al., 2021; Martinière et al., 2018; Rayle & Cleland, 1992; Savchenko et al., 2000).

The apoplast has a complex environment due to its structure, including the water-free space where the ion movement is not restricted by electrical charge, and the Donnan free space, which is characterized by the non-diffusible anion and associated to the cell wall (Bernstein & Nieman, 1960; Dainty & Hope, 1961; Richter & Dainty, 1989; Sattelmacher, 2001). This complexity creates a pH gradient in the apoplast, and the pH of the unstirred layer near the plasma membrane embedded with H^+ -ATPase and ion channels, such as K^+ channel, is expected to be higher than AF-pH (Martinière et al., 2018).

Root can be divided into different root zones, including root tip (covered by root cap), transition zone (or distal elongation zone), elongation zone, and maturation zone (or differentiation zone) (Baluška et al., 2001; Barrio et al., 2013; Ishikawa & Evans, 1995). Root cap covers the meristem zone, and can be divided into three regions, namely, inner cells, outer cells and root cap border cells (RBCs). As the root develops, the RBCs are sloughed off the meristematic cell, allowing meristematic cells to enter the transition zone to be initiated to elongate at a low rate (Baluška et al., 2001). In elongation zone, cells elongate at a higher rate to reach their maximum length. After reaching their length, elongated cells acquire their final differentiation state in the maturation zone (Ivanov & Dubrovsky, 2013). The different surface pH of different root zones were observed (Felle, 1998; Peters & Felle, 1999), suggesting there is a heterogeneity of AF-pH during root growth and development. However, AF-pH of each root zone has not yet been reported, as well as the dynamics of AF-pH during root growth and development.

Microelectrodes have been applied to measure the root apoplast pH at the cell wall surface (Jones et al., 1995; Peters & Felle, 1999). However, the microelectrode cannot access the inner region of the apoplast, being too large (microscale) to penetrate cell wall pores (nanoscale) (Carpita et al., 1979). This limitation makes it impractical to measure AF-pH using microelectrodes.

Fluorescent pH indicators are other means to quantitatively assess root apoplast pH. Using a microscope, the fluorescence signal of the indicators can be detected in deep tissues at the subcellular level, allowing researchers to monitor the apoplastic pH in plants

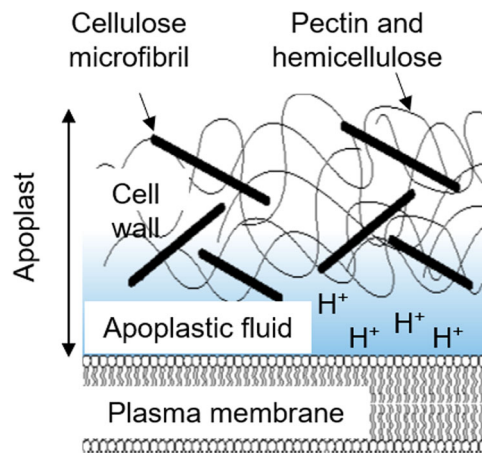


FIGURE 1 Schematic representation of root epidermal cell apoplast. Apoplast includes the cell wall and the apoplastic fluid on the outer plasma membrane. The cell wall is predominantly composed of cellulose, hemicellulose and pectin. The blue region represents the apoplastic fluid in the water-free space of the apoplast.

(Fendrych et al., 2016; Gjetting et al., 2012; Kesten et al., 2019; Martinière et al., 2018). Both chemical-based fluorescent indicators such as Oregon green (Fasano et al., 2001) and 8-hydroxypyrene-1,3,6-trisulfonic acid trisodium salt (HPTS) (Barbez et al., 2017) and genetically encoded indicators such as pHluorin (Miesenböck et al., 1998) and pHusion (Gjetting et al., 2012) have been applied to investigate root apoplastic pH (Gao et al., 2004; Gjetting et al., 2012; Martinière et al., 2018; Miesenböck et al., 1998). However, phototoxicity from the excitation light and photobleaching limit the application of fluorescent indicators when serial images need to be taken over time, including time-lapse imaging (Bernas et al., 2004; El-Esawi et al., 2017; Icha et al., 2017; Kutschera & Briggs, 2012; Song et al., 1996; Wright et al., 2002; Zhang et al., 2013). Blue light irradiation, which was used for excitation in previous reports (Barbez et al., 2017; Gao et al., 2004; Gjetting et al., 2012), also induces H^+ -ATPase activity on the plasma membrane of the guard cells (Inoue & Kinoshita, 2017; Kinoshita & Shimazaki, 1999; Martinière et al., 2018), which can lower the apoplastic pH by transporting the protons from the cytosol to the apoplast. Blue light also induces cytosolic Ca^{2+} increase in whole seedlings (Babourina et al., 2002; Baum et al., 1999; Zhao et al., 2013). This Ca^{2+} increase may lead to changes in apoplastic pH, as Ca^{2+} dynamics were reported to correlate with apoplastic pH (Gao et al., 2004; Martinière et al., 2018; Monshausen et al., 2009). This evidence suggests that fluorescence imaging has limitations when used for root AF-pH measurements requiring minimal perturbation to root homeostasis.

Genetically encoded bioluminescent indicators can be a better alternative for studies of root AF-pH. The luminescence signal of a bioluminescent indicator is produced by the oxidation of its substrate, which eliminates the requirement for excitation light in fluorescence imaging. Moreover, light emission from bioluminescent protein is much dimmer than that of fluorescence excitation (Choy et al., 2003),

which could reduce interference in plant physiological function (Icha et al., 2017). Indeed, there are no reports of bioluminescence-induced light toxicity in plants. Hence, bioluminescent proteins are useful for time-lapse imaging in roots. For example, firefly luciferases have been applied in studies of root branching or activities related to circadian rhythm (Bordage et al., 2016; Moreno-Risueno et al., 2010).

Several bioluminescent pH indicators have been generated, including the firefly-luciferase-based dual reporter system (Gabriel & Viviani, 2014), pHlash (Zhang et al., 2016) and Luphin (Nakamura et al., 2021). pHlash and Luphin are ratiometric pH indicators based on bioluminescence resonance energy transfer (BRET). Ratiometric bioluminescent indicators can indicate the pH by the change of emission ratio of the acceptor (fluorescent moiety) and the donor (luciferase), and this emission ratio is regardless of the change of bioluminescence intensity (Zhang et al., 2016). All of these, however, can only monitor pH in the range 5.4–9.0, which is not suitable for the acidic environment (pH 4.6–7.0) of the root apoplast (Barbez et al., 2017; Fasano et al., 2001; Geilfus, 2017; Gjetting et al., 2012; Martinière et al., 2018). In 2016, a bioluminescent protein, Green-enhanced Nano-lantern (GeNL) (Suzuki et al., 2016), was developed by fusing the luciferase NanoLuc (Nluc) (Hall et al., 2012) and the fluorescent protein mNeongreen (mNG) (Shaner et al., 2013). When Nluc catalyses the substrate oxidation, the substrate is in an excited state. The excited-state substrate then emits the bioluminescence, and at the same time, produces non-radiative energy. This energy then excites mNG non-radiatively through BRET. GeNL bioluminescence intensity was sufficient for subcellular live imaging at a time resolution of seconds in *Petunia hybrida* root (Tran et al., 2021), and it responded to pH changes between pH 5.0 and 8.0 in *A. thaliana* (Furuhata et al., 2020). These data suggest that GeNL can be used to monitor AF-pH. However, the expression of GeNL in the AF has not been investigated, and a detailed analysis of the GeNL emission spectrum at different pH levels is necessary before GeNL can be used for quantitative analysis of AF-pH in roots.

Using signal peptides may be a good strategy to precisely localise genetically encoded indicators in the AF. By fusing different signal peptides to pHluorin, localisation of this indicator in the endoplasmic reticulum (ER), trans-Golgi network, prevacuole and acid/lytic vacuole was achieved (Martinière et al., 2013). *A. thaliana* chitinase signal peptide was used to secrete pHusion into the extracellular space; however, the authors also observed non-specific localisation in the ER (Gao et al., 2004; Gjetting et al., 2012), which interferes with the interpretation of the apoplastic pH. Tobacco chitinase A signal peptide (Di Sansebastiano et al., 1998) was also used to induce secretion into the apoplast (Martinière et al., 2018). Although the apoplastic localisation was successful, only dim fluorescence was detected in the AF, which was insufficient for pH measurement. This might be due to the limitation of the pHluorin, which cannot indicate pH lower than pH 5.0. In light of these studies, a new signal peptide that can efficiently deliver pH indicator proteins to the apoplast is needed for precise AF-pH inspection.

An alternative method to localise genetically encoded indicators in the apoplast is to anchor them on the outside of the plasma

membrane facing the apoplast. Such approaches were done by attaching pHusion to the apoplastic side of the plasma membrane via fusion to the Sytaxin SYP122 protein (Kesten et al., 2019), or fusing pHluorin to the transmembrane domain of plasma membrane-localized TM23 (Brandizzi et al., 2002; Martinière et al., 2018). However, this approach can only measure the apoplastic pH near the plasma membrane but not the free AF.

A. thaliana endo-1,4- β -glucanase (Cel1), a cellulase with a predicted 25-amino acid signal peptide, is associated with cell wall thickening (Shani et al., 1997, 2006). In this study, we applied the Cel1 signal peptide to precisely deliver GeNL to the root AF and examined the reciprocal emission spectrum change of GeNL to quantify the AF-pH of *A. thaliana* root zones. Furthermore, we performed time-lapse imaging of the root and examined the influence of ambient pH changes on AF-pH to understand the dynamics of AF-pH and its homeostasis.

2 | MATERIALS AND METHODS

2.1 | Vector construction

GeNL was amplified from GeNL/pcDNA3 (Suzuki et al., 2016) with the forward primer 5'-AGC ATG CAT ATG GTG TCC AAG GGC GAAG-3' and reverse primer 5'-CAT GGA GCT CTT ACG CCA GAA TGC GTT CGC-3' to introduce *EcoT22I* and *SacI* restriction sites, respectively. PCR product was subsequently subcloned into the backbone vector 35S::AtADH1(AT1G77120)-UTR::HSP18.2/pUC19 by digestion with *EcoT22I* and *SacI* and ligation with T4 ligase (Promega). The backbone vector was a kind gift from Dr. Ko Kato of the Nara Institute of Science and Technology, Japan. The resulting 35S::AtADH1-UTR:GeNL::HSP18.2 cassette was subcloned into the binary vector pCAMBIA1301 (Cambia) by using *HindIII* and *EcoRI* restriction enzymes and by T4 DNA ligation (Promega).

For AF-targeted GeNL, the coding region of the signal peptide of *A. thaliana* endo-1,4- β -glucanase (Cel1) (GenID: 843408), 5'-ATG GCG CGA AAA TCC CTA ATT TTC CCG GTG ATT TTG CTC GCC GTT CTT CTC TTC TCT CCG CCG ATT TAC TCC GCC-3', was amplified from *A. thaliana* genomic DNA with forward primer 5'-AGC ATG CAT ATG GCG CGA AAA TCC CTA ATTT-3' for insertion of an *EcoT22I* restriction site and the reverse primer 5'-GGA CAC CAT GGC GGA GTA AAT CGG CCG A-3' that has a 9-bp overlap with GeNL. Overlap PCR was performed to insert the Cel1 signal peptide sequence at 5' end of GeNL. GeNL was amplified with 5'-TAC TCC GCC ATG GTG TCC AAG GGC GAA GA-3', which contains 9 bp of overlap with AtCel1 signal peptide, and reverse primer 5'-CAT GGA GCT CTT ACG CCA GAA TGC GTT CGC-3', designed to introduce the *SacI* restriction site. Overlap PCR with the forward primer 5'-AGC ATG CAT ATG GCG CGA AAA TCC CTA ATTT-3' and the reverse primer 5'-CATG GAG CTC TTA CGC CAG AAT GCG TTC GC-3' using a 1:100 diluted mixture of the first PCR product was performed to produce the final AtCel1SP-GeNL. The final PCR product was cloned into the 35S::AtADH1-UTR::HSP18.2/pUC19 vector and then

cloned into pCAMBIA1301 vector through a similar strategy with the 35S::GeNL::HSP18.2 construct using the same restriction sites.

2.2 | Plant materials and strain construction

The 35S::AtADH1-UTR:GeNL::HSP18.2/pCAMBIA1301 and 35S::AtADH1-UTR:AtCel1SP-GeNL::HSP18.2/pCAMBIA1301 vectors were introduced into GV3101 *Agrobacterium tumefaciens* by the heat shock protocol adopted from Höfgen and Willmitzer (1988). *A. thaliana* Columbia (Col-0) plants were transformed by floral dip method (Bent, 2006). Transgenic seeds were sowed on 0.8% agar/3% sucrose and half-strength Murashige and Skoog (MS) medium containing 20 mg/L hygromycin. Transgenic seedlings were screened with Invitrogen SAFE IMAGER BLUE-LIGHT TRANSIL. Selected seedlings with green fluorescence (emission 520 nm) were moved to the soil to grow and seeds were collected. Three heterozygous lines from the T₁ generation and one homozygous line from the T₂ generation of the 35S::AtADH1-UTR:AtCel1SP-GeNL::HSP18.2 (35S::Cel1SP-GeNL) line were obtained and analysed. The T₂ homozygous line was used as the representative for all 35S::Cel1SP-GeNL lines. Plants were grown in long-day conditions (16 h light/8 h night) at 21°C. For imaging experiments, seeds were sterilized with 20% antiformin with a few drops of 20% Triton X-100, vortexed for 7 min, rinsed with autoclaved water 2–3 times, and then placed on 0.8% agar/3% sucrose, pH 5.8, half-strength MS medium and grown vertically to create a flat root contact surface.

2.3 | Confocal microscopy

To observe the localisation of GeNL in the 35S::GeNL and 35S::Cel1SP-GeNL lines, fluorescence images of the leaf and root epidermis were taken with a Nikon A1 confocal microscope equipped with an eclipse Ti microscope and an S Fluor oil-immersion objective lens (magnification, ×40, ×60; numerical aperture, 1.30). The sample was placed flat between the slide glass and cover glass. For plasmolysed root cell fluorescence imaging, a 4- to 6-day-old seedling was submerged in 4 µg/ml FM4-64 0.5 M mannitol or 1 µg/ml propidium iodide (PI) 0.5 M mannitol solution for 3 min before imaging. The excitation wavelength of 488 nm was used for GeNL, Cel1SP-GeNL (emission filter 515/30), FM4-64, and PI fluorescence (emission filter 595/50). The excitation wavelength of 636 nm was used for chloroplast autofluorescence (emission filter 700/75). Fluorescence plot was analysed using ImageJ, Plot Profile function.

2.4 | In vitro spectroscopy of GeNL

To determine the pK_a of GeNL, recombinant GeNL protein purified from *Escherichia coli* was diluted from the PBS stock with trisodium

citrate and borax buffer following the procedure described by Zhao et al. (2011) to make the final 50 nM GeNL solutions at different pH levels from 4.0 to 7.5 with a 0.5 pH unit interval. One microlitre of furimazine solution (Promega) as substrate was added to 100 µl protein solution, and the emission spectrum was measured with the photonic multichannel analyser (PMA 12; Hamamatsu Photonics). Emission spectrum was measured from 400 to 750 nm (with a 5 nm unit interval).

2.5 | In vitro and in situ pH calibration of GeNL

For in vitro calibration, *E. coli* purified protein was diluted in PBS or half-strength MS medium at different pH levels (from 4.0 to 7.5 at 0.5 pH unit interval) containing 10 mM 2-(N-morpholino) ethanesulfonic acid (MES) and 10 mM citrate, as pH buffers for pH range from 4.0 to 7.5. Images were taken by Olympus inverted IX-83 microscope with two channels and electron-multiplying charge-coupled device (EMCCD) camera, with a 100-ms exposure time for each channel and specific bandpass filters corresponding to 460- or 520-nm emission in a darkroom. The 460 nm emission was detected with the U-FCFP 460–510 bandpass filter (Olympus), and the 520 nm emission was detected with the U-FBNA 510–550 bandpass filter (Olympus). The switching time of the filters between taking images in each channel was less than 1 s. The GeNL emission ratio was calculated by dividing the emission intensity at 520 nm by the emission intensity at 460 nm. To investigate the sensitivity of GeNL to K⁺ and Na⁺, stock GeNL was diluted to 3% sucrose half-strength MS medium containing 100 mM KCl, 100 mM NaCl, 10 mM Ca²⁺ or 10 mM Mg²⁺ to make the final 50 nM protein concentration. One microlitre of furimazine solution (Promega) as substrate was added to 100 µl protein solution. For in situ calibration, 35S::Cel1SP-GeNL *A. thaliana* roots were placed on a glass slide in half-strength MS medium at different pH levels (from 4.0 to 7.5 at 0.5 pH unit interval) containing 10 mM MES, 10 mM citrate buffers, and 0.01% Triton X-100, which enables permeation of buffer into the extracellular space, and 1% furimazine. Emission signals were measured by the same inverted microscope (IX-83, Olympus) with the same set-up as the in vitro calibration. The emission ratio of 520 nm/460 nm on the outline of each root zone cell within the region of interest (ROI) was calculated. From one image, five cells were selected from each root, and 4–5 roots were analysed. Averaged value of all cells was calculated to determine the AF-pH. The pH dependency of this ratio was analysed by the Hill's cooperativity model with a model function given by,

$$R = P \frac{K_a^n}{x^n + K_a^n} + Q \frac{x^n}{x^n + K_a^n},$$

where R is the 520 nm/460 nm emission ratio, n is the Hill coefficient, P is the high-pH limit of R, Q is the low-pH limit of R, x = 10^{-pH}, and K_a = 10^{-pK_a}. The least-squares fitting calculation was performed using Origin software (OriginLab Pro 8.1) to determine the pK_a value.

2.6 | Root bioluminescence time-lapse imaging

For time-lapse imaging of AF-pH in live *A. thaliana* root epidermis, we prepared a slide glass with a thin layer of pH 5.8 half-strength MS medium (liquid medium). For imaging with *35S::Cel1SP-GeNL* *A. thaliana*, a 4- to 5-day-old seedling was placed in the pH 5.8 half-strength MS medium and gently agitated 3–5 times to remove the external Cel1SP-GeNL protein that accumulates on the root surface. The sample was incubated for 20 min at room temperature in pH 5.8 half-strength MS medium, then a cover glass was placed on top of the root. Before imaging, pH 5.8 half-strength MS medium was replaced with an imaging medium (pH 5.8 half-strength MS medium with 1% furimazine) by slowly fusing the imaging medium to the slide glass while removing the pH 5.8 half-strength MS medium. We placed the tip of a folded kimwipe in between the cover glass and slide glass to slowly absorb the pH 5.8 half-strength MS medium on one side of the cover glass, while adding 100 μ l of the same medium containing 1% furimazine by a pipette from the other side. We confirmed that the substrate concentration was saturated during the whole imaging process, as bioluminescence of a new *35S::Cel1SP-GeNL* root sample can be detected when placed in the used medium. The same procedure was followed for imaging using MES and citrate buffered imaging medium. For different pH medium treatments, the pH levels of the media were adjusted to the desired values with HCl or KOH. Images were acquired in the same conditions as for the in situ calibration experiments for 35 min, with a 2-s exposure time for each

channel, maximum EM gain, and no interval time with fixed imaging stage. Data were collected and analysed with Metamorph software (Molecular Device). Ratio images were captured using the “Ratio images” function with the intensity based on the FF01-520/35 bandpass filter image. The kymograph and velocity of bioluminescence cluster in the *35S::Cel1SP-GeNL* root was generated using the kymograph function. “Best fit range” and “AutoScale” functions were applied to adjust the intensity of each frame in the supplementary videos.

2.7 | Statistical analysis

Statistical analysis was conducted using Student's *t*-test using Microsoft Excel.

3 | RESULTS

3.1 | In vitro analysis confirmed GeNL as a bioluminescent ratiometric pH indicator

We assessed the function of the GeNL protein as a bioluminescent ratiometric pH indicator by measuring the GeNL emission spectrum in response to the pH change (Figure 2a). The ratio of GeNL emission at 520 nm to its emission at 460 nm increased from pH 4.0 to 7.5,

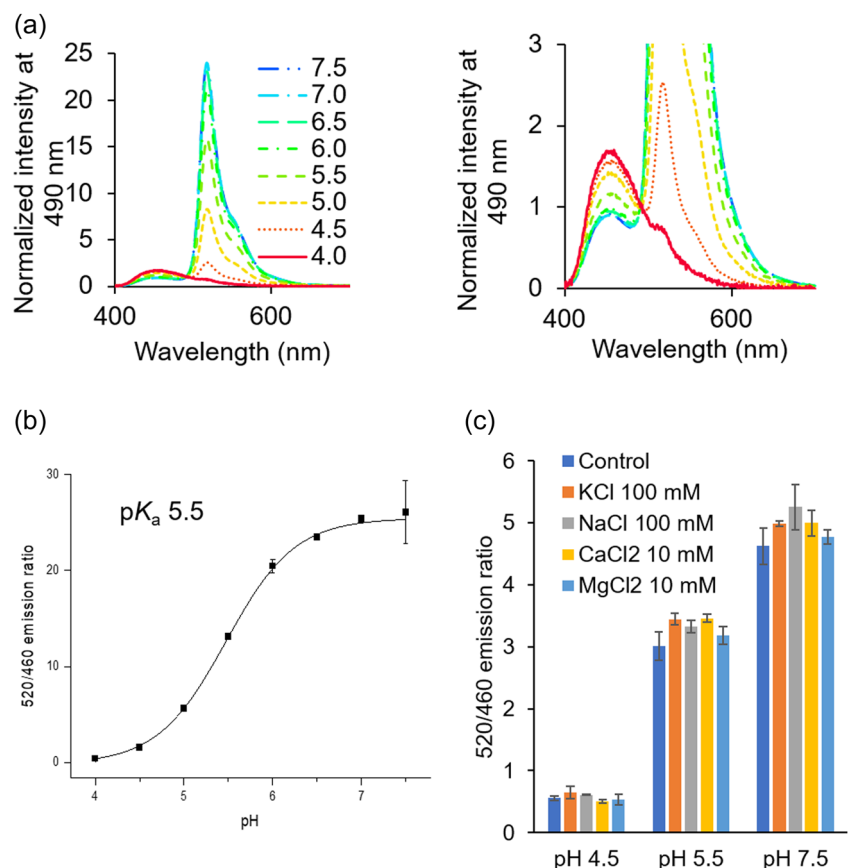


FIGURE 2 Response of purified GeNL to different pH and ion concentrations. (a) (left) Bioluminescence emission spectrum of purified GeNL from *Escherichia coli* in PBS buffer at pH from 4.0 to 7.5 (0.5 pH unit intervals). Bioluminescence intensity was normalized to 490 nm emission intensity. (right) Scale-adjusted bioluminescence emission spectrum using the same data. (b) In vitro calibration of purified GeNL emission ratio (520 nm/460 nm) in PBS buffer. (c) mNG/Nluc emission ratio of GeNL in different ion concentrations (mM) in half-strength MS medium at pH 4.5, 5.5 and 7.5. Error bars are \pm standard deviation (SD) ($n = 5$). GeNL, Green-enhanced Nano-lantern; MS, Murashige and Skoog.

with a pK_a of 5.5 (Figure 2b). We also assessed the GeNL emission ratio in half-strength MS, as this medium was later used for in vivo analyses. The dynamic range was unaffected; however, the pK_a of the GeNL emission ratio shifted to 6.0 (Supporting Information: Figure 1S). To further investigate how pH affects the GeNL emission ratio, we assessed the GeNL fluorescence and Nluc bioluminescence intensity in half-strength MS medium in response to pH change. The GeNL fluorescence intensity increased from pH 4.0 to 7.5 (Supporting Information: Figure 2S) with pK_a of 5.9, displaying a similar pH dependency with the ratio calculated from the GeNL bioluminescence (Supporting Information: Figure 1S), whereas the Nluc bioluminescence intensity (without mNG) displayed lower pK_a of 5.0 (Supporting Information: Figure 3S). GeNL emission ratio in half-strength MS medium was not affected by the change of K^+ , Ca^{2+} , Na^+ , Mg^{2+} or Cl^- ions concentrations (Figure 2c), which indicates that the change of ion concentration in the root apoplast will not affect the performance of GeNL as a pH indicator during imaging. The results demonstrated that GeNL could be a useful pH indicator around pH 4.5–6.5, which is within the range for AF-pH measurement.

3.2 | Fusion of AtCel1 signal peptide to GeNL confers apoplast localisation

To localise GeNL in the apoplast, we fused the predicted signal peptide of *A. thaliana* Cel1 to the N terminus of GeNL to yield Cel1SP-GeNL (Figure 3a) and ubiquitously expressed this transgene in *A. thaliana* by using the CaMV 35S promoter. Fluorescence imaging with a confocal laser scanning microscope confirmed the localisation of Cel1SP-GeNL and GeNL in *A. thaliana*. In leaf and root epidermis, we detected GeNL fluorescence in the cytoplasm, whereas Cel1SP-GeNL fluorescence overlapped with the cell outline (Figure 3b), suggesting successful secretion of Cel1SP-GeNL into the apoplast.

To further clarify the cell localisation of GeNL and Cel1SP-GeNL, we treated the root with PI, which stains the cell wall (Figure 3c), or with FM4-64, which stains the plasma membrane (Figure 3d) (Vida & Emr, 1995), and then plasmolysed the cells to shrink the protoplast to expand the space between the cell wall and the plasma membrane. PI can diffuse into the root apoplast (Naseer et al., 2012) and bind to the pectin in the cell wall (Rounds et al., 2011). Hence, the PI fluorescence can represent the cell wall, an effect that we used to visualise the root epidermis cell wall (Figure 3c). Furthermore, Cel1SP-GeNL was localised in the space outside of the plasma membrane, without any detectable fluorescence in the cytoplasm (lower panels of Figure 3c, d). In contrast, without Cel1 signal peptide, we observed GeNL fluorescence in the cytoplasm, but not in the extracellular space (Figure 3b–d). Furthermore, higher magnification and line plot showed that Cel1SP-GeNL fluorescence was not detected in the cell wall region (Figure 3e, f), suggesting Cel1SP-GeNL did not diffuse into or bind to the cell wall. We also generated protoplasts from 35S::GeNL and 35S::Cel1SP-GeNL line and inspected the fluorescence of Cel1SP-GeNL (520 nm) to confirm whether Cel1SP-GeNL fluorescence is retained in the cytoplasm. As expected,

no fluorescence was detected in the 35S::Cel1SP-GeNL protoplast, whereas fluorescence was detected in 35S::GeNL that does not have the Cel1 signal peptide (Supporting Information: Figure 4S). Therefore, we believe that by using the Cel1 signal peptide, we successfully localised GeNL in the AF.

We also took macroscale images of 35S::Cel1SP-GeNL and 35S::GeNL lines and found that the 35S::GeNL line displayed green bioluminescence, as expected, while the bioluminescence colour of the 35S::Cel1SP-GeNL line shifted to cyan-green (Figure 3g). The emission spectrum of the 35S::GeNL line showed a single peak at 520 nm, with a very small shoulder from 450 to 500 nm. By contrast, the 35S::Cel1SP-GeNL line showed an additional peak at around 460 nm (Supporting Information: Figure 5S). This change in bioluminescence emission spectrum and visible colour may be due to the difference in pH between the apoplast and the cytoplasm. To note, there were no obvious differences in the root growth rate and morphology between the 35S::Cel1SP-GeNL seedlings in comparison to the wildtype (Supporting Information: Figure 6S).

3.3 | Cel1SP-GeNL fusion protein enables visualisation of AF

Next, we performed time-lapse observations of bioluminescence in root cells from the 35S::Cel1SP-GeNL line and observed clear movement of the bioluminescence signal along the apoplast of the main root maturation zone (Supporting Information: Video 1S, left panel). The minimum temporal resolution achieved in this experimental condition was 3 s. By comparison, we did not see any movement of the bioluminescence signal in the main root of the 35S::GeNL line (Supporting Information: Video 1S, right panel). We observed slow movement in the root hairs of the 35S::GeNL line (Supporting Information: Video 1S). To determine the direction and velocity of the bioluminescence stream, we generated a kymograph of the bioluminescence cluster observed in the maturation zone of the root in the 35S::Cel1SP-GeNL line (Figure 4), from which we determined that the velocity of the stream in the main root was $0.97 \pm 0.06 \mu\text{m s}^{-1}$. The velocities of the bioluminescence streams in root hairs of 35S::Cel1SP-GeNL and 35S::GeNL lines were 1.47 ± 0.05 and $0.20 \pm 0.04 \mu\text{m s}^{-1}$, respectively. Cel1SP-GeNL bioluminescence allowed visualisation of the AF flow at a time resolution of seconds, which showed a higher velocity than the fluid flow in the cytoplasm.

3.4 | Quantitative pH imaging in Arabidopsis root reveals pH differences between root zones

Finally, we investigated the capability of GeNL as a pH indicator for the imaging of AF-pH dynamics in roots. We observed similar pH profiles in four independent lines (Supporting Information: Figure 7S), so we used a homozygous 35S::Cel1SP-GeNL line as the representative sample for the rest of the study. For image acquisition, raw images in both 460 and 520 nm were taken alternatively, with 2 s exposure time

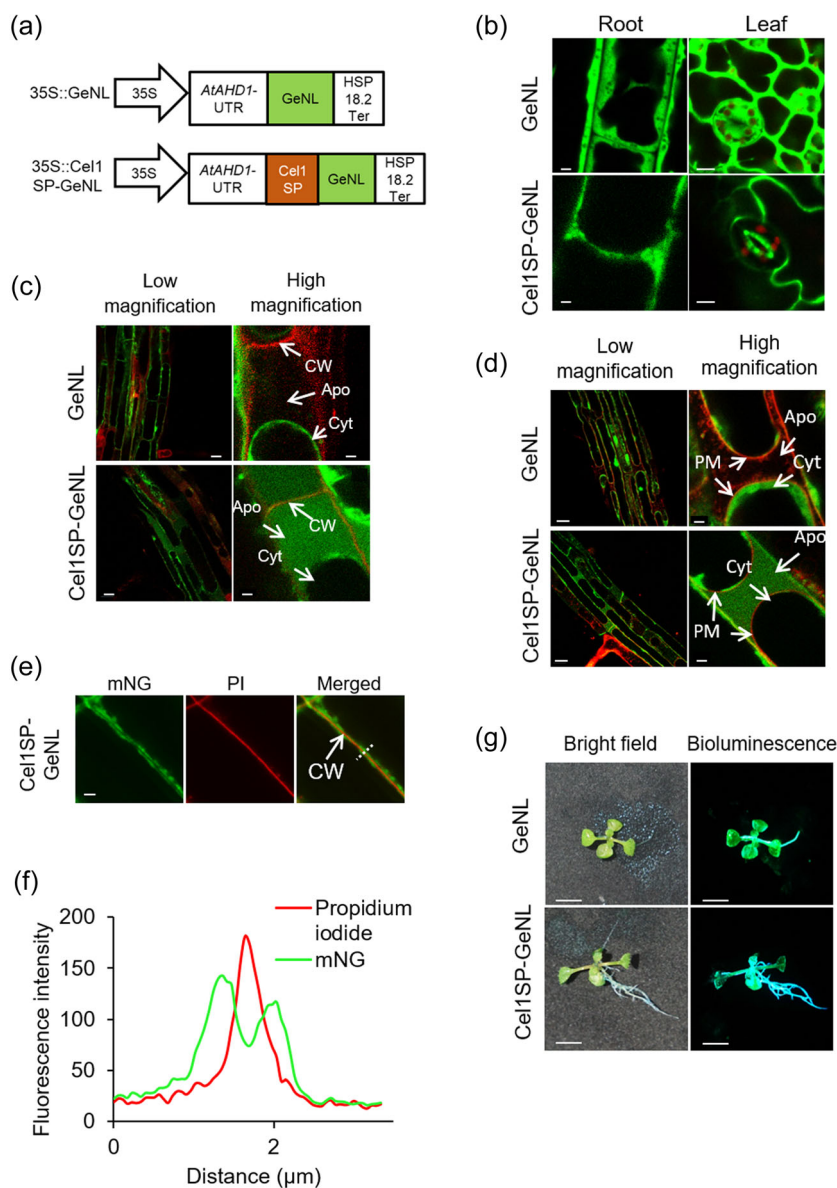


FIGURE 3 Expression and localisation of GeNL and Cel1SP-GeNL in *Arabidopsis*. (a) Schematic representation of the expression cassettes used for 35S::GeNL and 35S::Cel1SP-GeNL transformation. (b) Fluorescence images of 35S::GeNL and 35S::Cel1SP-GeNL leaves and roots. Overlaid image of fluorescence from the green fluorescent moiety mNeonGreen (mNG; green) of Cel1SP-GeNL and GeNL, and chloroplast autofluorescence (red) showing the localisation of GeNL in the guard cell of leaf epidermis. Scale bars: 1 μ m in root images (left panels), 10 μ m in leaf images (right panels). (c) Fluorescent images of 35S::GeNL and 35S::Cel1SP-GeNL roots stained with PI and treated with 500 mM mannitol. GeNL and Cel1SP-GeNL fluorescence (green) were detected in the cytoplasm and apoplast, respectively. The cell wall was stained with PI (red). Scale bars: low magnification (left panels), 10 μ m; high magnification (right panels), 1 μ m. (d) Fluorescent images of 35S::GeNL and 35S::Cel1SP-GeNL roots stained with FM4-64 and treated with 500 mM mannitol. GeNL and Cel1SP-GeNL fluorescence (green) were detected in the cytoplasm and apoplast, respectively. The plasma membrane was stained with FM4-64 (red). Scale bars: low magnification (left panels), 10 μ m; high magnification (right panels), 1 μ m. (e) Fluorescence images of 35S::Cel1SP-GeNL root cell. Cell wall was stained with propidium iodide (PI) (red). The fluorescence of mNeonGreen (mNG) at 520 nm (green) did not overlap with PI fluorescence (red), suggesting Cel1SP-GeNL was not localised in the cell wall. Scale bars: 2 μ m. (f) Line plot analysis of mNG (green) and PI (red) fluorescence along the white dashed line in (e), indicating that the fluorescence of mNG and PI does not overlap. (g) Images of 35S::Cel1SP-GeNL and 35S::GeNL seedlings 2 weeks after germination, showing the green bioluminescence of the 35S::GeNL line shifted to cyan-green in the 35S::Cel1SP-GeNL line. Apo, apoplast; CW, cell wall; Cyt, cytoplasm; PM, plasma membrane.

of each channel (plus few seconds to switch filters). Therefore, it required about 7 s for each frame of ratio image, which was the highest temporal resolution under our experimental condition. In vitro calibration with purified GeNL using a microscope was performed,

showing pK_a of 5.5 (Supporting Information: Figure 8S). The dynamic range decreased as expected because the filter band in the microscope system was broader compared to the photonic multichannel analyser, but the same pK_a was achieved (Figure 1). This data confirmed that

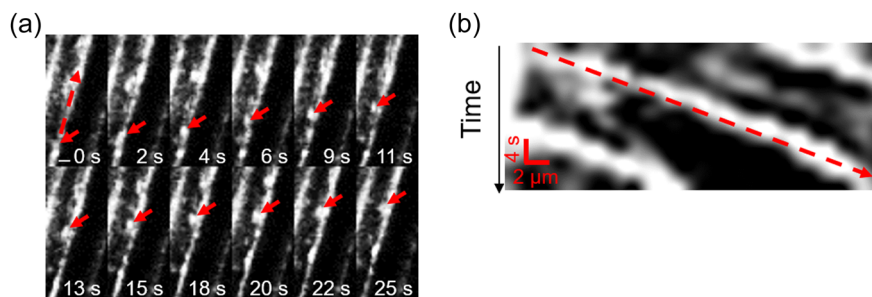


FIGURE 4 Root apoplastic fluid flow indicated by Cel1SP-GeNL bioluminescence. (a) Montage of time-lapse images of the bioluminescence cluster in the 35S::Cel1SP-GeNL root. Red arrows indicate the location of a bioluminescence cluster. Scale bar: 5 μm . (b) Kymograph of the bioluminescence cluster in (a). The distance and direction were indicated by a red dashed arrow in the top left panel of (a). Red arrowhead indicates the distance and direction. A time-lapse video of this figure can be seen in Supporting Information: Video 1S.

measurement of GeNL emission ratio from images taken by a microscope can be applied. For calculation of AF-pH in plant, we calibrated the GeNL bioluminescence emission ratio of 35S::Cel1SP-GeNL root cells in different pH medium, as the Cel1SP-GeNL may behave differently with *E. coli* purified GeNL and the apoplast environment may affect the Cel1SP-GeNL function. We took images of the root from the 35S::Cel1SP-GeNL line after placing it in pH 4.5–7.5 half-strength MS medium containing 10 mM MES, 10 mM citrate pH buffers, and a surfactant, Triton X-100 (Figure 5a), to enable the buffer to permeate into the extracellular space. Only cells in the epidermal layers (the outermost layer of cells on both sides of the root) of the elongation zone that are in direct contact to the buffer were measured (Figure 5a). From the images, we then plotted the 520 nm/460 nm emission ratios to obtain an in situ calibration curve of Cel1SP-GeNL, which showed a pK_a of 5.7 (Figure 5b). All of the calculation of the root AF-pH was based on the in situ calibration (Figure 5b).

Next, to confirm the performance of Cel1SP-GeNL as a pH indicator in the root apoplast, we used fusicoccin to induce the acidification in the root apoplast and measured the AF-pH. Fusicoccin is known to activate the H^+ -ATPase and decrease the AF-pH (Barbez et al., 2017; Johansson et al., 1993). Similar with the previous report (Barbez et al., 2017), 35S::Cel1SP-GeNL root displayed lower AF-pH compared to the non-treated root (Figure 5c). This result confirmed that Cel1SP-GeNL can indicate the pH of root apoplast.

Next, we compared AF-pH in different root zones of the 35S::Cel1SP-GeNL line (Figure 6a). We found that each root zone had different AF-pH, which decreases in the order of root cap that covers the whole meristematic zone (pH 5.7), elongation zone where cells are elongating to reach their maximum length (pH 5.4), and the maturation zone where cells are developing into different root tissues, including root hair and lateral root (pH 5.3) (Figure 6b). We also compared whether the ROI selected from a single cell or a wider region of a root zone had any influence on the ratio. No significant difference between the ROIs was observed, indicated by the similar 520 nm/460 nm emission ratio (Figure 6B). Since roots develop from the meristematic zone (covered with root cap) towards the elongation

zone and maturation zone, these results suggested that the AF-pH in root acidifies as the root elongates and develops.

3.5 | Time-lapse pH imaging shows dynamic acidification during root development

To clarify the acidification of AF during root development, we performed time-lapse imaging of different root zones during development and quantified the AF-pH (Supporting Information: Video 2S). The averaged AF-pH of single cells and the whole region (Figure 6b) was similar (Supporting Information: Figure 9S). We found that AF-pH in the root acidified as the roots developed: Approximately pH 5.7 at the cells of the root cap, around pH 5.4 at the cells of the elongation zone, and near pH 5.2 at the cells of the maturation zone (Supporting Information: Table 1S). While the AF-pH in the maturation zone remained unchanged, the AF-pH of the root cap and elongation zone decreased after 25 min of growth (Figure 6c, Supporting Information: Table 1S, Video 2S).

To understand the effects of ambient pH on AF-pH dynamics in relation to root growth, we examined the AF-pH dynamics of the elongation zone at different medium pH levels. The AF-pH of the root elongation zone in pH 4.5 was higher than that in pH 5.8 and 7.5 media; however, the pace of pH decrease of the root elongation zone in pH 4.5 and 7.5 media was similar to that in pH 5.8 medium (Figure 7, Supporting Information: Figure 10S, Table 2S). Although root elongation was observed in the pH 4.5 and 5.8 media, root growth was inhibited in the pH 7.5 medium (Supporting Information: Video 3S). The root growth inhibition at pH 7.5 indicated that the root is responding to the increased ambient pH. These results showed that the root elongation zone is regulated to lower the AF-pH regardless of different ambient pH, even when the root growth is inhibited by high ambient pH.

Since our results reported that the root AF-pH differs from the medium pH, we hypothesized that the root apoplast has a buffering ability to regulate the root AF-pH against higher/lower medium pH. To investigate this, we examined the root AF-pH in different medium

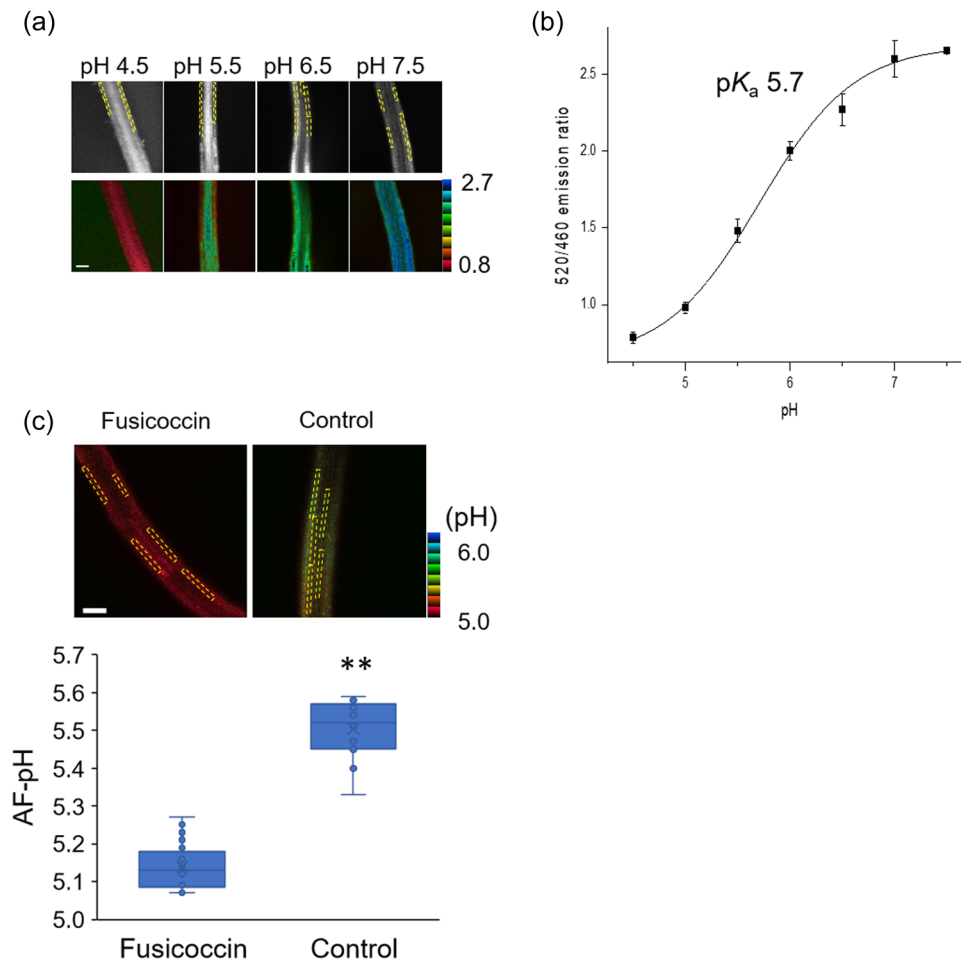


FIGURE 5 In situ calibration with *35S::Cel1SP-GeNL* roots. (a) Ratio images of *35S::Cel1SP-GeNL* root in pH 4.5, 5.5, 6.5 and 7.5 half-strength MS medium. Lookup table represents the 520 nm/460 nm emission ratio range of 0.8–2.7. Scale bars: 50 μ m. White dashed box: region of interest (ROI) used for pH measurement. (b) In situ calibration of the GeNL emission ratio (520 nm/460 nm) of the *35S::Cel1SP-GeNL* root in half-strength MS medium at pH 4.5–7.5 (at intervals of 0.5 pH units). Error bars: \pm SD ($n = 25$). (c) Representative images and calculation of the AF-pH of root elongation zone under 5 μ M fusicoccin treatment. Scale bars: 50 μ m. Asterisks indicate significant difference using Student's *t* test with $p < 0.01$ ($n = 25$).

pH levels with MES and citrate buffer. These buffers are expected to neutralize the pH of the root apoplast regulated by the proton pumps (H^+ -ATPase), which has been reported to antagonize the auxin-induced alkalization when it is activated by fusicoccin (Li et al., 2021). The root AF-pH in the buffered pH 7.5 medium was higher than that in pH 4.5 and 5.8, and the root AF-pH did not decrease over time (25 min), unlike the root AF-pH in the non-buffered media (Supporting Information: Figures 11S, 12S, Table 3S).

4 | DISCUSSION

4.1 | Apoplast localisation with novel AtCel1 signal peptide

By fusing GeNL with a novel signal peptide of Cel1, we successfully obtained secretion of Cel1SP-GeNL into the

apoplast. Our data showed no detectable Cel1SP-GeNL fluorescence in the ER or cytoplasm, such as when the *A. thaliana* chitinase signal peptide was used (Gao et al., 2004). Notably, the Cel1 signal peptide contains a hydrophobic region (Shani et al., 1997). Protein folding is restricted when the hydrophobic region is tethered to the ER (Yan & Wu, 2014); this might inhibit Cel1SP-GeNL function and result in a lack of signal when Cel1SP-GeNL is temporarily located in the ER. The possibility of Cel1SP-GeNL localisation in the lytic vacuole cannot be excluded; in this case, the loss of Cel1SP-GeNL signal might be due to the acidic environment and the hydrolytic enzymes in the plant vacuole (Hara-Nishimura & Hatsugai, 2011; Matsuoka et al., 1997; Wu et al., 2000). Nevertheless, by using the constitutive 35S promoter, we achieved a sufficient Cel1SP-GeNL concentration in the extracellular space for AF-pH monitoring. This novel Cel1 signal peptide may also be applied to other indicators to monitor ions such as Ca^{2+} , K^+ or auxin in the extracellular space.

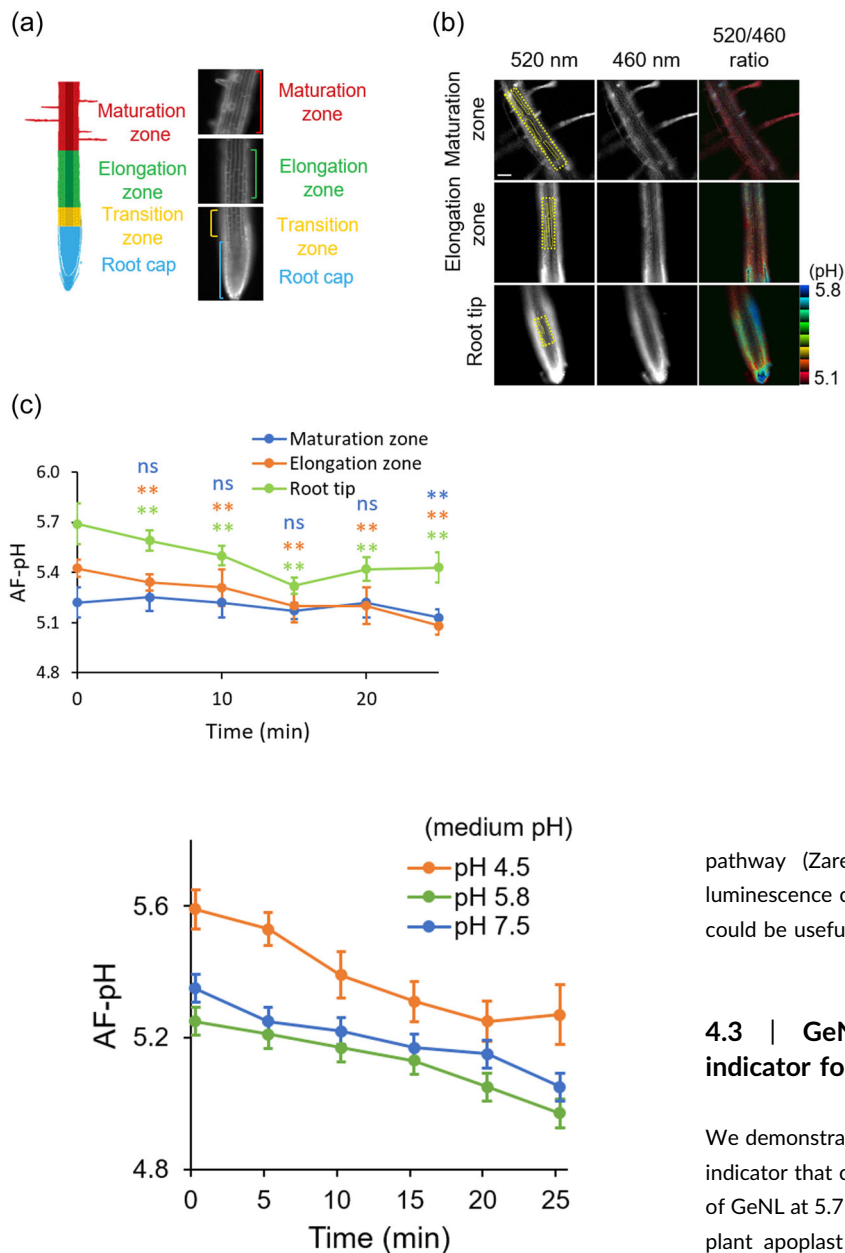


FIGURE 7 AF-pH dynamics of the 35S::Cel1SP-GeNL root elongation zone in media at different pH. (a) AF-pH of the elongation zone of the 35S::Cel1SP-GeNL root in pH 4.5, 5.8 and 7.5 half-strength MS medium. Error bars are \pm SD. The AF-pH of root in pH 5.8 medium was compared to the root in pH 4.5 and 7.5 medium for each time point by Student's *t* test. Significant difference was seen for all time points at $p < 0.01$ ($n = 25$).

4.2 | Dynamics of AF

To our knowledge, this is the first time that the AF flow in the root epidermis has been visualised at subcellular resolution. We observed faster movement of AF (using Cel1SP-GeNL) compared to cytosolic fluid (using GeNL). Similarly, in *Lupinus albus* root, the velocity of water uptake via the apoplastic pathway is higher than the symplastic

FIGURE 6 AF-pH dynamics of 35S::Cel1SP-GeNL root zones. (a) Schematic representation and representative bioluminescence images of *Arabidopsis thaliana* root zones. (b) Ratio images of different zones of 35S::Cel1SP-GeNL root. Lookup table represents pH 5.4–7.5. Scale bars: 50 μ m. Yellow dashed box: Region of interest (ROI) for pH measurement. (c) AF-pH of different root zones of the 35S::Cel1SP-GeNL root over 25 min. Error bars are \pm SD. Student's *t* test was performed to compare the AF-pH between 0 min and all other time points for each root zone. Asterisks indicate significant difference with AF-pH at $p < 0.01$; ns, not significant ($n = 25$). EZC, elongation zone cell; MZC, maturation zone cell; RCC, root cap cell.

pathway (Zarebanadkouki et al., 2019). As Cel1SP-GeNL bioluminescence could successfully represent the AF flow, this method could be useful for investigating AF dynamics in roots.

4.3 | GeNL as a bioluminescent ratiometric pH indicator for plant apoplast

We demonstrated the performance of GeNL as a bioluminescent pH indicator that can be used for monitoring the AF-pH. The in situ pK_a of GeNL at 5.7 could be a better choice for the acidic environment of plant apoplast that could reach below 5.0 compared to previous indicators such as pHusion (pK_a 6.0) or pHluorin (pK_a 7.0) (Bibikova et al., 1998; Gjetting et al., 2012; Kesten et al., 2019; Martinière et al., 2018; Rayle & Cleland, 1992; Shao et al., 2020). Both moieties of GeNL, Nluc and mNG, can function at pH lower than 5.0, especially Nluc with pK_a at 4.3, this feature might explain the ability of GeNL to indicate pH better in the range of 4.5–5.0 compared to previous indicators.

The pK_a of GeNL emission ratio overlapped with the pK_a of GeNL fluorescence intensity, suggesting that the change of the GeNL emission ratio correlates with the protonation of the mNG moiety, but not with the emission of Nluc. This result shows GeNL as a ratiometric pH indicator, which can avoid the bias of intensimetric-type indicators caused by different protein concentration or protein accumulation. Furthermore, we demonstrated the measurement of pH decrease upon fusicoccin treatment, agreeing with previous reports (Barbez et al., 2017; Li et al., 2021), which supports that Cel1SP-GeNL can be useful for monitoring the AF-pH.

GeNL is a bioluminescent indicator, which needs its substrate, furimazine, to luminesce. Therefore, for bioluminescence imaging using GeNL in plants, substrate delivery or substrate penetration to the tissue of interest needs to be considered. In this and previous studies, the substrate could penetrate into root apoplast or cytoplasm (Tran et al., 2021) of the epidermal cells by absorption. However, in other tissues (e.g. flower, leaf or stem), the substrate has to penetrate through the wax/cuticle layers, and surfactants such as Triton-X100 or dimethyl sulfoxide (DMSO) is used (Tran et al., 2021), which may become destructive. Non-destructive substrate delivery methods, such as cargo-encapsulated substrate for plant, will need to be investigated for over hours-long in situ imaging.

Here, we showed that GeNL can function as a ratiometric pH indicator. The pH-dependent emission of GeNL correlated strongly to the pH dependency of the mNG emission signal that has a similar pK_a . We observed a change of bioluminescence intensity during the imaging process. However, in GeNL, BRET efficiency depends on the proximity, orientation and protonation of protein, but it is not influenced by the substrate availability. Therefore, the luminescence intensity does not influence the emission ratio of BRET-based ratiometric indicators, as seen in pHlash (Zhang et al., 2016). However, the decrease of intensity is also an important factor for bioluminescence imaging, as it will affect the spatio-temporal resolution.

4.4 | Heterogeneity of root AF-pH during elongation

Using Cel1SP-GeNL, we could observe the heterogeneity and acidity of the AF in all root zones. The root AF-pH of the elongation zone and maturation zone are in the range of 5.1–5.4, which is similar to previous reports (Bibikova et al., 1998; Kesten et al., 2019). As the meristematic zone was covered by the root cap, we were unable to monitor its AF-pH. Further examination of root cap ablation could be conducted to precisely measure the meristematic AF-pH that locates underneath (Shi et al., 2018; Tsugeki & Fedoroff, 1999).

4.5 | Regulation of root AF-pH against ambient pH change

AF-pH in the elongation zone of the root epidermis was different with the ambient pH. This finding supports a previous report (Martinière et al., 2018) that also observed homeostasis of pH in the outer plasma membrane surface in roots during growth and development. From our data, we speculate that the AF in the root elongation zone, which was previously thought to be affected by ambient pH due to free diffusion of outside water and solutes into the apoplast, may be tightly regulated to maintain its pH. Regulation of pH might be facilitated by the proton-exporting activity of the H^+ -ATPase (AHA1 and AHA2) in the plasma membrane, which is known to be required for plant growth in ambient alkaline conditions (Falhof

et al., 2016; Haruta et al., 2010, 2017; Li et al., 2021) and regulated by the apoplastic pH (Fuglsang et al., 2007). The use of pH buffers such as MES or citrate might disrupt this regulation as demonstrated in this study and another report (Kesten et al., 2019), suggesting there may be a pH buffering activity in the root apoplast. The homeostasis of AF-pH might be essential for stable root growth, especially in the elongation zone where cells expand rapidly.

The cell wall can also be a protective barrier; it contains calcium-crosslinked homogalacturonan, which limits the diffusion of the external solution into the cell (Amos & Mohnen, 2019). At neutral or alkaline pH, cell elongation may be inhibited due to enhanced homogalacturonan chelation (Lootens et al., 2003; Phyo et al., 2019), which can occur regardless of the AF-pH. Our data agree with this hypothesis, as it shows that the ambient pH at 7.5 can inhibit root elongation. Further investigation of cell wall pH dynamics should be conducted to elucidate the relationship between plasma membrane pH, AF-pH, and cell wall pH in response to ambient pH changes. Investigation of apoplastic and cytosolic Ca^{2+} dynamics in parallel with pH will also help elucidate the role of Ca^{2+} in apoplastic pH homeostasis, as Ca^{2+} concentration is associated with the apoplastic pH (Gao et al., 2004).

In conclusion, our data provide evidence of the acidic environment of root AF-pH, supporting the acid growth theory. By demonstrating the maintenance of AF-pH against ambient pH change, our data support the existence of root apoplastic pH homeostasis, established by an as yet unknown mechanism, that protects the root from the outside environment.

ACKNOWLEDGEMENTS

We are grateful to Dr. Ko Kato from the Nara Institute of Science and Technology, Japan, for gifting us the plant expression cassette vector and to Dr. Hidehiro Fukaki from Kobe University, Japan, for his valuable comments on our study. This study was supported by a Grant-in-Aid for Scientific Research for Houga of Japan Society for the Promotion of Science (JSPS) (17K19525 to T. N.), the SENTAN program of Japan science and technology agency (No. 16812798 to T. N.), the Plant Transgenic Design Initiative (PTraD)-2017 of the Gene Research Center, the Tsukuba-Plant Innovation Research Center, the University of Tsukuba [16KEIGI A1-23, 17KEIGI A-21 to T. N.], and a scholarship from the Ministry of Education, Culture, Sports, Science, and Technology of Japan (MEXT) to Q. T.

CONFLICT OF INTEREST

The authors declare no conflict of interest.

DATA AVAILABILITY STATEMENT

The data that support the findings of this study are available from the corresponding author upon reasonable request.

ORCID

Quang Tran  <http://orcid.org/0000-0001-9609-6737>

Takeharu Nagai  <http://orcid.org/0000-0003-2650-9895>

REFERENCES

- Amos, R.A. & Mohnen, D. (2019) Critical review of plant cell wall matrix polysaccharide glycosyltransferase activities verified by heterologous protein expression. *Frontiers in Plant Science*, 10, 915. Available from: <https://doi.org/10.3389/fpls.2019.00915>
- Babourina, O., Newman, I. & Shabala, S. (2002) Blue light-induced kinetics of H⁺ and Ca²⁺ fluxes in etiolated wild-type and phototropin-mutant *Arabidopsis* seedlings. *Proceedings of the National Academy of Sciences of the United States of America*, 99, 2433–2438. Available from: <https://doi.org/10.1073/pnas.042294599>
- Baluška, F., Volkmann, D. & Barlow, P.W. (2001) A polarity crossroad in the transition growth zone of maize root apices: cytoskeletal and developmental implications. *Journal of Plant Growth Regulation*, 20, 170–181. Available from: <https://doi.org/10.1007/s003440010013>
- Barbez, E., Dünser, K., Gaidora, A., Lendl, T. & Busch, W. (2017) Auxin steers root cell expansion via apoplastic pH regulation in *Arabidopsis thaliana*. *Proceedings of the National Academy of Sciences of the United States of America*, 114, E4884–E4893. Available from: <https://doi.org/10.1073/pnas.1613499114>
- Barrio, R.A., Romero-Arias, J.R., Noguez, M.A., Azpeitia, E., Ortiz-Gutiérrez, E., Hernández-Hernández, V. et al. (2013) Cell patterns emerge from coupled chemical and physical fields with cell proliferation dynamics: the *Arabidopsis thaliana* root as a study system. *PLoS Computational Biology*, 9, e1003026. Available from: <https://doi.org/10.1371/journal.pcbi.1003026>
- Baum, G., Long, J.C., Jenkins, G.I. & Trewavas, A.J. (1999) Stimulation of the blue light phototropic receptor NPH1 causes a transient increase in cytosolic Ca²⁺. *Proceedings of the National Academy of Sciences of the United States of America*, 96, 13554–13559. Available from: <https://doi.org/10.1073/pnas.96.23.13554>
- Bent, A. (2006) *Arabidopsis thaliana* floral dip transformation method. In: Wang, K. (Ed.) *Agrobacterium protocols*. Totowa, NJ: Humana Press, pp. 87–104. Available at: <https://doi.org/10.1385/1-59745-130-4:87>
- Bernas, T., Zarebski, M., Dobrucki, J.W. & Cook, P.R. (2004) Minimizing photobleaching during confocal microscopy of fluorescent probes bound to chromatin: role of anoxia and photon flux. *Journal of Microscopy*, 215, 281–296. Available from: <https://doi.org/10.1111/j.0022-2720.2004.01377.x>
- Bernstein, L. & Nieman, R.H. (1960) Apparent free space of plant roots. *Plant Physiology*, 35, 589–598. Available from: <https://doi.org/10.1104/pp.35.5.589>
- Bibikova, T.N., Jacob, T., Dahse, I. & Gilroy, S. (1998) Localized changes in apoplastic and cytoplasmic pH are associated with root hair development in *Arabidopsis thaliana*. *Development*, 125, 2925–2934. Available from: <https://doi.org/10.1242/dev.125.15.2925>
- Bordage, S., Sullivan, S., Laird, J., Millar, A.J. & Nimmo, H.G. (2016) Organ specificity in the plant circadian system is explained by different light inputs to the shoot and root clocks. *New Phytologist*, 212, 136–149. Available from: <https://doi.org/10.1111/nph.14024>
- Brandizzi, F., Frangne, N., Marc-Martin, S., Hawes, C., Neuhaus, J.-M. & Paris, N. (2002) The destination for single-pass membrane proteins is influenced markedly by the length of the hydrophobic domain. *The Plant Cell*, 14, 1077–1092. Available from: <https://doi.org/10.1105/tpc.000620>
- Carpita, N., Sabulase, D., Montezinos, D. & Delmer, D.P. (1979) Determination of the pore size of cell walls of living plant cells. *Science*, 205, 1144–1147. Available from: <https://doi.org/10.1126/science.205.4411.1144>
- Choy, G., O'Connor, S., Diehn, F.E., Costouros, N., Alexander, H.R., Choyke, P. et al. (2003) Comparison of noninvasive fluorescent and bioluminescent small animal optical imaging. *Biotechniques*, 35(1022–1026), 1028–1030. Available from: <https://doi.org/10.2144/03355rr02>
- Dainty, J. & Hope, A. (1961) The electric double layer and the Donnan equilibrium in relation to plant cell walls. *Australian Journal of Biological Sciences*, 14, 541–551. Available from: <https://doi.org/10.1071/B19610541>
- Di Sansebastiano, G.P., Paris, N., Marc-Martin, S. & Neuhaus, J.M. (1998) Specific accumulation of GFP in a non-acidic vacuolar compartment via a C-terminal propeptide-mediated sorting pathway. *Plant Journal*, 15, 449–457. Available from: <https://doi.org/10.1046/j.1365-313x.1998.00210.x>
- El-Esawi, M., Arthaut, L.-D., Jourdan, N., d'Harlingue, A., Link, J., Martino, C.F. et al. (2017) Blue-light induced biosynthesis of ROS contributes to the signaling mechanism of *Arabidopsis* cryptochrome. *Scientific Reports*, 7, 13875. Available from: <https://doi.org/10.1038/s41598-017-13832-z>
- Elmore, J.M. & Coaker, G. (2011) The role of the plasma membrane H⁺-ATPase in plant–microbe interactions. *Molecular Plant*, 4, 416–427. Available from: <https://doi.org/10.1093/mp/ssq083>
- Falhof, J., Pedersen, J.T., Fuglsang, A.T. & Palmgren, M. (2016) Plasma membrane H⁺-ATPase regulation in the center of plant physiology. *Molecular Plant*, 9, 323–337. Available from: <https://doi.org/10.1016/j.molp.2015.11.002>
- Fasano, J.M., Swanson, S.J., Blancaflor, E.B., Dowd, P.E., Kao, T.H. & Gilroy, S. (2001) Changes in root cap pH are required for the gravity response of the *Arabidopsis* root. *The Plant Cell*, 13, 907–921. Available from: <https://doi.org/10.1105/tpc.13.4.907>
- Felle, H.H. (1998) The apoplastic pH of the *Zea mays* root cortex as measured with pH-sensitive microelectrodes: aspects of regulation. *Journal of Experimental Botany*, 49, 987–995. Available from: <https://doi.org/10.1093/jxb/49.323.987>
- Fendrych, M., Leung, J. & Friml, J. (2016) TIR1/AFB-Aux/IAA auxin perception mediates rapid cell wall acidification and growth of *Arabidopsis* hypocotyls. *eLife*, 5, e19048. Available from: <https://doi.org/10.7554/eLife.19048>
- Fuglsang, A.T., Guo, Y., Cui, T.A., Qiu, Q., Song, C., Kristiansen, K.A. et al. (2007) *Arabidopsis* protein kinase PKS5 inhibits the plasma membrane H⁺-ATPase by preventing interaction with 14-3-3 protein. *The Plant Cell*, 19, 1617–1634. Available from: <https://doi.org/10.1105/tpc.105.035626>
- Furuhata, Y., Sakai, A., Murakami, T., Nagasaki, A. & Kato, Y. (2020) Bioluminescent imaging of *Arabidopsis thaliana* using an enhanced Nano-lantern luminescence reporter system. *PLoS One*, 15, e0227477. Available from: <https://doi.org/10.1371/journal.pone.0227477>
- Gabriel, G.V.M. & Viviani, V.R. (2014) Novel application of pH-sensitive firefly luciferases as dual reporter genes for simultaneous ratiometric analysis of intracellular pH and gene expression/location. *Photochemical & Photobiological Sciences*, 13, 1661–1670. Available from: <https://doi.org/10.1039/c4pp00278d>
- Gao, D., Knight, M.R., Trewavas, A.J., Sattelmacher, B. & Plieth, C. (2004) Self-reporting *Arabidopsis* expressing pH and [Ca²⁺] indicators unveil ion dynamics in the cytoplasm and in the apoplast under abiotic stress. *Plant Physiology*, 134, 898–908. Available from: <https://doi.org/10.1104/pp.103.032508>
- Geilfus, C.M. (2017) The pH of the apoplast: dynamic factor with functional impact under stress. *Molecular Plant*, 10, 1371–1386. Available from: <https://doi.org/10.1016/j.molp.2017.09.018>
- Gjetting, S.K., Ytting, C.K., Schulz, A. & Fuglsang, A.T. (2012) Live imaging of intra- and extracellular pH in plants using pHusion, a novel genetically encoded biosensor. *Journal of Experimental Botany*, 63, 3207–3218. Available from: <https://doi.org/10.1093/jxb/ers040>
- Hall, M.P., Unch, J., Binkowski, B.F., Valley, M.P., Butler, B.L., Wood, M.G. et al. (2012) Engineered luciferase reporter from a deep sea shrimp utilizing a novel imidazopyrazinone substrate. *ACS Chemical Biology*, 7, 1848–1857. Available from: <https://doi.org/10.1021/cb3002478>
- Hara-Nishimura, I. & Hatsugai, N. (2011) The role of vacuole in plant cell death. *Cell Death & Differentiation*, 18, 1298–1304. Available from: <https://doi.org/10.1038/cdd.2011.70>

- Haruta, M., Tan, L.X., Bushey, D.B., Swanson, S.J. & Sussman, M.R. (2017) Environmental and genetic factors regulating localization of the plant plasma membrane H⁺-ATPase. *Plant Physiology*, 176, 364–377. Available from: <https://doi.org/10.1104/pp.17.01126>
- Haruta, M., Burch, H.L., Nelson, R.B., Barrett-Wilt, G., Kline, K.G., Mohsin, S.B. et al. (2010) Molecular characterization of mutant Arabidopsis plants with reduced plasma membrane proton pump activity. *Journal of Biological Chemistry*, 285, 17918–17929. Available from: <https://doi.org/10.1074/jbc.M110.101733>
- Höfgen, R. & Willmitzer, L. (1988) Storage of competent cells for Agrobacterium transformation. *Nucleic Acids Research*, 16, 9877. Available from: <https://doi.org/10.1093/nar/16.20.9877>
- Icha, J., Weber, M., Waters, J.C. & Norden, C. (2017) Phototoxicity in live fluorescence microscopy, and how to avoid it. *BioEssays*, 39, 39. Available from: <https://doi.org/10.1002/bies.201700003>
- Inoue, S.-I. & Kinoshita, T. (2017) Blue light regulation of stomatal opening and the plasma membrane H⁺-ATPase. *Plant Physiology*, 174, 531–538. Available from: <https://doi.org/10.1104/pp.17.00166>
- Ishikawa, H. & Evans, M.L. (1995) Specialized zones of development in roots. *Plant Physiology*, 109, 725–727. Available from: <https://doi.org/10.1104/pp.109.3.725>
- Ivanov, V.B. & Dubrovsky, J.G. (2013) Longitudinal zonation pattern in plant roots: conflicts and solutions. *Trends in Plant Science*, 18, 237–243. Available from: <https://doi.org/10.1016/j.tplants.2012.10.002>
- Johansson, F., Sommarin, M. & Larsson, C. (1993) Fusicoccin activates the plasma membrane H⁺-ATPase by a mechanism involving the C-terminal inhibitory domain. *The Plant Cell*, 5, 321–327. Available from: <https://doi.org/10.1105/tpc.5.3.321>
- Jones, D.L., Shaff, J.E. & Kochian, L.V. (1995) Role of calcium and other ions in directing root hair tip growth in *Limnium stoloniferum*. *Planta*, 197, 672–680. Available from: <https://doi.org/10.1007/BF00191575>
- Kesten, C., Gámez-Arjona, F.M., Menna, A., Scholl, S., Dora, S., Huerta, A.I. et al. (2019) Pathogen-induced pH changes regulate the growth-defense balance in plants. *The EMBO Journal*, 38, e101822. Available from: <https://doi.org/10.15252/embj.2019101822>
- Kinoshita, T. & Shimazaki, K.-I. (1999) Blue light activates the plasma membrane H⁺-ATPase by phosphorylation of the C-terminus in stomatal guard cells. *The EMBO Journal*, 18, 5548–5558. Available from: <https://doi.org/10.1093/emboj/18.20.5548>
- Kutschera, U. & Briggs, W.R. (2012) Root phototropism: from dogma to the mechanism of blue light perception. *Planta*, 235, 443–452. Available from: <https://doi.org/10.1007/s00425-012-1597-y>
- Li, L., Verstraeten, I., Roosjen, M., Takahashi, K., Rodriguez, L., Merrin, J. et al. (2021) Cell surface and intracellular auxin signalling for H⁺ fluxes in root growth. *Nature*, 599, 273–277. Available from: <https://doi.org/10.1038/s41586-021-04037-6>
- Lootens, D., Capel, F., Durand, D., Nicolai, T., Boulenguer, P. & Langendorff, V. (2003) Influence of pH, Ca concentration, temperature and amidation on the gelation of low methoxyl pectin. *Food Hydrocolloids*, 17, 237–244. Available from: [https://doi.org/10.1016/S0268-005X\(02\)00056-5](https://doi.org/10.1016/S0268-005X(02)00056-5)
- Martinière, A., Bassil, E., Jublanc, E., Alcon, C., Reguera, M., Sentenac, H. et al. (2013) In vivo intracellular pH measurements in tobacco and Arabidopsis reveal an unexpected pH gradient in the endomembrane system. *The Plant Cell*, 25, 4028–4043. Available from: <https://doi.org/10.1105/tpc.113.116897>
- Martinière, A., Gibrat, R., Sentenac, H., Dumont, X., Gaillard, I. & Paris, N. (2018) Uncovering pH at both sides of the root plasma membrane interface using noninvasive imaging. *Proceedings of the National Academy of Sciences of the United States of America*, 115, 6488–6493. Available from: <https://doi.org/10.1073/pnas.1721769115>
- Matsuoka, K., Higuchi, T., Maeshima, M. & Nakamura, K. (1997) A vacuolar-type H⁺-ATPase in a nonvacuolar organelle is required for the sorting of soluble vacuolar protein precursors in tobacco cells. *The Plant Cell*, 9, 533–546. Available from: <https://doi.org/10.1105/tpc.9.4.533>
- Miesenböck, G., De Angelis, D.A. & Rothman, J.E. (1998) Visualizing secretion and synaptic transmission with pH-sensitive Green fluorescent proteins. *Nature*, 394, 192–195. Available from: <https://doi.org/10.1038/28190>
- Monshausen, G.B., Bibikova, T.N., Weisenseel, M.H. & Gilroy, S. (2009) Ca²⁺ regulates reactive oxygen species production and pH during mechanosensing in Arabidopsis roots. *The Plant Cell*, 21, 2341–2356. Available from: <https://doi.org/10.1105/tpc.109.068395>
- Moreno-Risueno, M.A., Van Norman, J.M., Moreno, A., Zhang, J., Ahnert, S.E. & Benfey, P.N. (2010) Oscillating gene expression determines competence for periodic Arabidopsis root branching. *Science*, 329, 1306–1311. Available from: <https://doi.org/10.1126/science.1191937>
- Nakamura, S., Fu, N., Kondo, K., Wakabayashi, K.I., Hisabori, T. & Sugiura, K. (2021) A luminescent Nanoluc-GFP fusion protein enables readout of cellular pH in photosynthetic organisms. *Journal of Biological Chemistry*, 296, 100134. Available from: <https://doi.org/10.1074/jbc.RA120.016847>
- Naseer, S., Lee, Y., Lapierre, C., Franke, R., Nawrath, C. & Geldner, N. (2012) Casparian strip diffusion barrier in Arabidopsis is made of a lignin polymer without suberin. *Proceedings of the National Academy of Sciences of the United States of America*, 109, 10101–10106. Available from: <https://doi.org/10.1073/pnas.1205726109>
- Peters, W.S. & Felle, H.H. (1999) The correlation of profiles of surface pH and elongation growth in maize roots. *Plant Physiology*, 121, 905–912. Available from: <https://doi.org/10.1104/pp.121.3.905>
- Phyo, P., Gu, Y. & Hong, M. (2019) Impact of acidic pH on plant cell wall polysaccharide structure and dynamics: insights into the mechanism of acid growth in plants from solid-state NMR. *Cellulose*, 26, 291–304. Available from: <https://doi.org/10.1007/s10570-018-2094-7>
- Rayle, D.L. & Cleland, R.E. (1992) The Acid Growth Theory of auxin-induced cell elongation is alive and well. *Plant Physiology*, 99, 1271–1274. Available from: <https://doi.org/10.1104/pp.99.4.1271>
- Richter, C. & Dainty, J. (1989) Ion behavior in plant cell walls. II. Measurement of the Donnan free space, anion-exclusion space, anion-exchange capacity, and cation-exchange capacity in delignified *Sphagnum russowii* cell walls. *Canadian Journal of Botany*, 67, 460–465. Available from: <https://doi.org/10.1139/b89-064>
- Rounds, C.M., Lubeck, E., Hepler, P.K. & Winship, L.J. (2011) Propidium iodide competes with Ca(2+) to label pectin in pollen tubes and Arabidopsis root hairs. *Plant Physiology*, 157, 175–187. Available from: <https://doi.org/10.1104/pp.111.182196>
- Sattelmacher, B. (2001) The apoplast and its significance for plant mineral nutrition. *New Phytologist*, 149, 167–192. Available from: <https://doi.org/10.1046/j.1469-8137.2001.00034.x>
- Savchenko, G., Wiese, C., Neimanis, S., Hedrich, R. & Heber, U. (2000) pH regulation in apoplastic and cytoplasmic cell compartments of leaves. *Planta*, 211, 246–255. Available from: <https://doi.org/10.1007/s004250000280>
- Shaner, N.C., Lambert, G.G., Chammass, A., Ni, Y., Cranfill, P.J., Baird, M.A. et al. (2013) A bright monomeric green fluorescent protein derived from *Branchiostoma lanceolatum*. *Nature Methods*, 10, 407–409. Available from: <https://doi.org/10.1038/nmeth.2413>
- Shani, Z., Dekel, M., Tsabary, G. & Shoseyov, O. (1997) Cloning and characterization of elongation specific endo-1,4-β-glucanase (cel1) from *Arabidopsis thaliana*. *Plant Molecular Biology*, 34, 837–842. Available from: <https://doi.org/10.1023/a:1005849627301>
- Shani, Z., Dekel, M., Roiz, L., Horowitz, M., Kolosovski, N., Lapidot, S. et al. (2006) Expression of endo-1,4-β-glucanase (cel1) in *Arabidopsis thaliana* is associated with plant growth, xylem development and cell wall thickening. *Plant Cell Reports*, 25, 1067–1074. Available from: <https://doi.org/10.1007/s00299-006-0167-9>

- Shao, Q., Gao, Q., Lhamo, D., Zhang, H. & Luan, S. (2020) Two glutamate- and pH-regulated Ca²⁺ channels are required for systemic wound signaling in *Arabidopsis*. *Science Signaling*, 13, eaba1453. Available from: <https://doi.org/10.1126/scisignal.aba1453>
- Shi, C.-L., von Wangenheim, D., Herrmann, U., Wildhagen, M., Kulik, I., Kopf, A. et al. (2018) The dynamics of root cap sloughing in *Arabidopsis* is regulated by peptide signalling. *Nature Plants*, 4, 596–604. Available from: <https://doi.org/10.1038/s41477-018-0212-z>
- Song, L., Varma, C.A., Verhoeven, J.W. & Tanke, H.J. (1996) Influence of the triplet excited state on the photobleaching kinetics of fluorescein in microscopy. *Biophysical Journal*, 70, 2959–2968. Available from: [https://doi.org/10.1016/S0006-3495\(96\)79866-1](https://doi.org/10.1016/S0006-3495(96)79866-1)
- Suzuki, K., Kimura, T., Shinoda, H., Bai, G., Daniels, M.J., Arai, Y. et al. (2016) Five colour variants of bright luminescent protein for real-time multicolour bioimaging. *Nature Communications*, 7, 13718. Available from: <https://doi.org/10.1038/ncomms13718>
- Tran, Q., Osabe, K., Entani, T. & Nagai, T. (2021) A novel petal up-regulated PhXTH7 promoter analysis in *Petunia hybrida* by using bioluminescence reporter gene. *Plant Biotechnology*, 38, 197–204. Available from: <https://doi.org/10.5511/plantbiotechnology.21.0130a>
- Tsugeki, R. & Fedoroff, N.V. (1999) Genetic ablation of root cap cells in *Arabidopsis*. *Proceedings of the National Academy of Sciences of the United States of America*, 96, 12941–12946. Available from: <https://doi.org/10.1073/pnas.96.22.12941>
- Vida, T.A. & Emr, S.D. (1995) A new vital stain for visualizing vacuolar membrane dynamics and endocytosis in yeast. *Journal of Cell Biology*, 128, 779–792. Available from: <https://doi.org/10.1083/jcb.128.5.779>
- Walter, A., Silk, W.K. & Schurr, U. (2000) Effect of soil pH on growth and cation deposition in the root tip of *Zea mays* L. *Journal of Plant Growth Regulation*, 19, 65–76. Available from: <https://doi.org/10.1007/p100021160>
- Wright, A., Bubb, W.A., Hawkins, C.L. & Davies, M.J. (2002) Singlet oxygen-mediated protein oxidation: evidence for the formation of reactive side chain peroxides on tyrosine residues. *Photochemistry and Photobiology*, 76, 35–46. Available from: [https://doi.org/10.1562/0031-8655\(2002\)076%3C0035:sompoe%3E2.0.co;2](https://doi.org/10.1562/0031-8655(2002)076%3C0035:sompoe%3E2.0.co;2)
- Wu, M.M., Llopis, J., Adams, S., McCaffery, J.M., Kulomaa, M.S., Machen, T.E. et al. (2000) Organelle pH studies using targeted avidin and fluorescein-biotin. *Chemical Biology*, 7, 197–209. Available from: [https://doi.org/10.1016/s1074-5521\(00\)00088-0](https://doi.org/10.1016/s1074-5521(00)00088-0)
- Yan, S. & Wu, G. (2014) Signal peptide of cellulase. *Applied Microbiology and Biotechnology*, 98, 5329–5362. Available from: <https://doi.org/10.1007/s00253-014-5742-3>
- Zarebanadkouki, M., Trtik, P., Hayat, F., Carminati, A. & Kaestner, A. (2019) Root water uptake and its pathways across the root: quantification at the cellular scale. *Scientific Reports*, 9, 12979. Available from: <https://doi.org/10.1038/s41598-019-49528-9>
- Zhang, K.-X., Xu, H.-H., Yuan, T.-T., Zhang, L. & Lu, Y.-T. (2013) Blue-light-induced PIN3 polarization for root negative phototropic response in *Arabidopsis*. *The Plant Journal*, 76, 308–321. Available from: <https://doi.org/10.1111/tjp.12298>
- Zhang, Y., Robertson, J.B., Xie, Q. & Johnson, C.H. (2016) Monitoring intracellular pH change with a genetically encoded and ratiometric luminescence sensor in yeast and mammalian cells. *Methods in Molecular Biology*, 1461, 117–130. Available from: https://doi.org/10.1007/978-1-4939-3813-1_9
- Zhao, X., Wang, Y.-L., Qiao, X.-R., Wang, J., Wang, L.-D., Xu, C.-S. et al. (2013) Phototropins function in high-intensity blue light-induced hypocotyl phototropism in *Arabidopsis* by altering cytosolic calcium. *Plant Physiology*, 162, 1539–1551. Available from: <https://doi.org/10.1104/pp.113.216556>
- Zhao, Y., Araki, S., Wu, J., Teramoto, T., Chang, Y.F., Nakano, M., Abdelfattah, A.S., 2011) An expanded palette of genetically encoded Ca²⁺ indicators. *Science*, 333, 1888–1891. Available from: <https://doi.org/10.1126/science.1208592>

SUPPORTING INFORMATION

Additional supporting information can be found online in the Supporting Information section at the end of this article.

How to cite this article: Tran, Q., Osabe, K., Entani, T., Wazawa, T., Hattori, M. & Nagai, T. (2022) Application of Green-enhanced Nano-lantern as a bioluminescent ratiometric indicator for measurement of *Arabidopsis thaliana* root apoplastic fluid pH. *Plant, Cell & Environment*, 45, 3157–3170. <https://doi.org/10.1111/pce.14404>